Proceedings of Global Power and Propulsion Society
ISSN-Nr: 2504-4400
GPPS Chania22
18th–20th September, 2022

www.gpps.global

GPPS-TC-2022-102

Large-Eddy Simulation of a Linear Compressor Cascade with Tip Flow: Effects of the Moving Endwall on the Aerodynamics

Lorenzo Becherucci, Régis Koch, Stéphane Moreau
Université de Sherbrooke
Becherucci.Lorenzo@USherbrooke.ca
2500 Boulevard de l'Université, Sherbrooke, J1K 2R1, QC, Canada

ABSTRACT

A wall-resolved compressible Large-Eddy Simulation of a linear compressor cascade with a moving end-wall has been performed with the high-order unstructured solver AVBP in order to study the effects of the wall motion on the tip-leakage flow aerodynamics. The cascade is composed of eight controlled diffusion airfoils with a tip-gap of 1.6% chord and a pitch-to-chord ratio of 0.925. The inflow Mach number is 0.07 and the Reynolds number based on the chord is 3.88×10^6. The moving end-wall moves in the pitchwise direction with a velocity magnitude that is 90.8% of the freestream inflow velocity. The main fluid-dynamic structures as the Tip-Leakage Vortex (TLV) and the wake have been resolved. Finally, a comparison between the current case and a previous simulation with a stationary end-wall has been done in order to investigate the effects of the wall motion in details. The TLV is flattened and entrained by the wall motion, resulting in a modified trajectory of the vortex. Moreover, this is characterized by lower turbulent kinetic energy. The aerodynamic comparison between the two cases sets the stage for a consistent aeroacoustic analysis.

INTRODUCTION

The secondary flow passing through the necessary gap existing between a rotor blade and the casing end-wall has been studied both experimentally and numerically over the last decades in order to understand the flow topology and evaluate the associated losses that lead to a decrease in the turbomachines efficiency. The flow is forced to cross the gap by the pressure difference between the pressure side (PS) and the suction side (SS) of the blade leading to the formation of a jet (Storer and Cumpsty, 1993), which, by interacting and mixing with the main streamwise flow in the passage rolls up in a coherent structure called Tip Leakage Vortex (TLV). Moreover, a Tip Separation Vortex (TSV) and a Counter Rotating Vortex (CRV) are also generated. The former is due to separation of the flow along the tip surface of the blade, while the latter comes from the interaction between the TLV and the boundary layer at the casing wall. All of these flow structures are responsible for pressure losses (Denton, 1993), blockage, stall inception and broadband noise emission (Kameier and Neise, 1997; Jacob et al., 2010; Koch et al., 2021*b*), which are all relevant to the overall performances of a turbofan engine.

Yet, as noted by Moreau (2022), the flow field around a turbofan blade is still too complex with for instance a strong interaction between a leading-edge vortex and the tip flow at approach (Kholodov and Moreau, 2020*a*) or a shock-boundary layer-tip vortices interaction in the tip region at cutback (Kholodov and Moreau, 2020*b*), to clearly assess the contributions of the tip vortices to losses and noise. Several physical features such as the cascade effect and the tip flow, need to be tackled independently, to decipher the modifications they induce on the flow and the radiated sound. The linear compressor cascade case considered here provides such an intermediate step. This configuration has been numerically investigated by You et al. (2004, 2006, 2007*b*) using an incompressible Large Eddy Simulation (LES) and an immersed boundary technique in the tip gap, while a more recent wall-resolved compressible LES on an unstructured body-fitted mesh in the tip clearance has been performed by Koch et al. (2021*a*,*b*). In the latter, the TLV dynamics was fully resolved and the effects of the boundary layer developing on the suction side evaluated. The present study analyzes and shows the effects of a moving end-wall on the TLV behaviour. It provides the first compressible wall-resolved LES performed on this configuration, experimentally investigated in Wang and Devenport (2004), and is meant to provide the basis for the subsequent acoustic study.

METHODOLOGY

Experimental Configuration

The experimental facility is the linear compressor cascade studied in Wang and Devenport (2004) and a sketch is shown in Fig.1. The cascade is composed of eight blades with a chord of 254 mm, and the profiles of which match the near tip region airfoil of the General Electric core-compressor rotor B (Wisler, 1977). They are mounted with a stagger angle of 56.9° and a pitch of 235 mm. The spanwise dimension is 250 mm and the tip-gap is 1.6% chord (4 mm). The inflow velocity magnitude is 25.5 m/s with an inlet angle of 65.1°, which leads to an angle of attack of 8.2°. The moving end-wall system involves a belt that slides over the lower end-wall of the cascade in the pitchwise direction with a velocity magnitude that is 90.8% of the freestream inflow velocity. More details on the experimental setup can be found in Muthanna and Devenport (2004); Wang and Devenport (2004); Wenger et al. (2004).

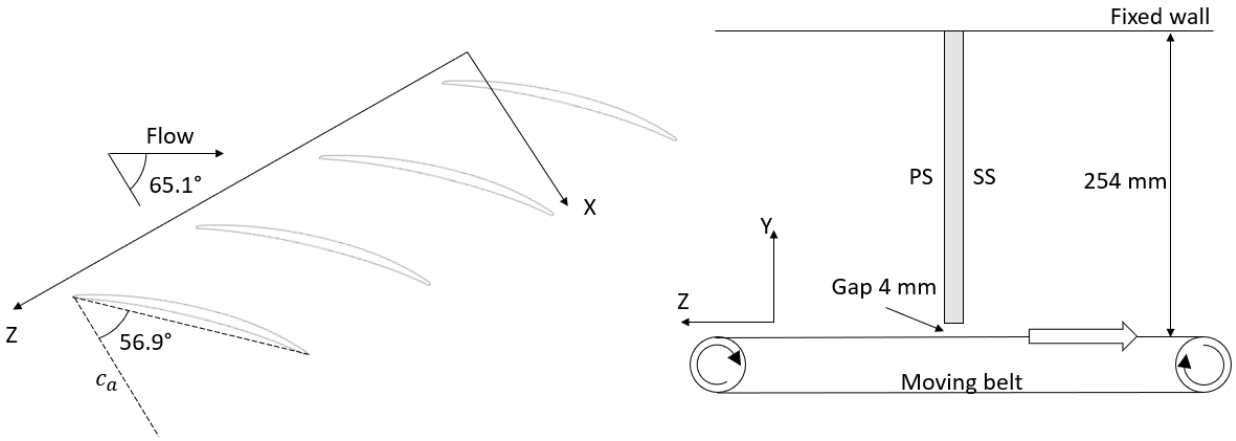

Figure 1 Sketch of the experimental facility.

Numerical Setup

The LES is performed with the compressible solver AVBP v7.9 developed at CERFACS (Schönfeld and Rudgyard, 1999). The computational domain shown in Fig.2 only involves one flow passage to limit the computational cost. The lateral boundaries along the Z direction are treated with periodicity conditions, whereas characteristic non-reflective boundary conditions (Poinsot and Lelef, 1992) are assigned to both inlet and outlet in order to avoid spurious reflections inside the domain (Odier et al., 2019). The lower plate is an adiabatic wall moving along the negative Z direction, while the upper plate is a slip wall. The implementation and validation of the new boundary condition to obtain the desired wall motion has been achieved in (Becherucci et al., 2022). The numerical scheme used is the explicit Two-step Taylor Galerkin 4A (TTG4A) scheme (Donea, 1984), which is third order in space and fourth order in time. In order to have the proper turbulence decay toward the walls, the sub-grid scale model used is the Wall-Adapting Local Eddy-viscosity model (WALE) (Nicoud and Ducros, 1999). The simulation time-step is set to 2.0 x 10^{-8}, which leads to a maximum CFL number of 0.7. The unstructured hybrid grid used for the present simulation is the same that has been created and shown in detail in Koch et al. (2021*a*). The mesh is composed of around 120 x 10^6 elements and is refined around the blade, in the near wake, and in the tip region (40 points along the spanwise direction with prismatic cells), in order to resolve most of the turbulent structures.

A trip similar to the experimental one is generated on the blade SS by randomly removing elements from the mesh as explained in Koch et al. (2021*a*). This device is used in the experiments to force and control the boundary layer transition. The simulation has been initialized with the LES solution from Koch et al. (2021*a*), so that an exponential ramp of 4 ms was imposed to let the wall reaching the wanted velocity. The simulation has run for 4.5 flow-through times (almost 45 ms) on the supercomputer Niagara from Compute Canada, using 40 nodes, each with 40 Intel Skylake cores at 2.4 GHz. The local convergence has been verified with different pressure probes. The temporal evolution of the pressure obtained on the blade SS at midspan, together with the evolution of the minimum, mean and maximal values for the pressure and temperature over the entire computational domain, is plotted in Fig. 3.

RESULTS AND DISCUSSION

0.1 Flow topology

Instantaneous iso-surfaces of Q criterion (with value $1.0 \times 10^6\ s^{-2}$) coloured by the velocity magnitude are shown in Fig. 4. The TLV is clearly seen at the tip of the blade. Its trajectory is qualitatively indicated with the white dashed line for both configurations with and without the sliding end-wall. The vortex in the current LES is clearly entrained by the wall towards the pressure side of the adjacent blade and it grows less in the spanwise direction, as will be shown in detail in the

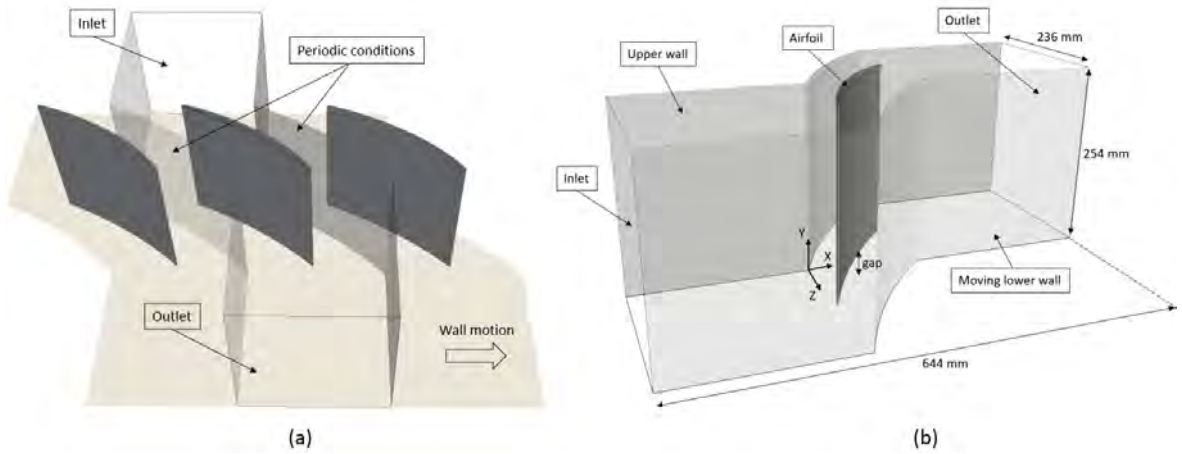

Figure 2 Numerical domain - (a): compressor cascade; (b): single passage and reference system.

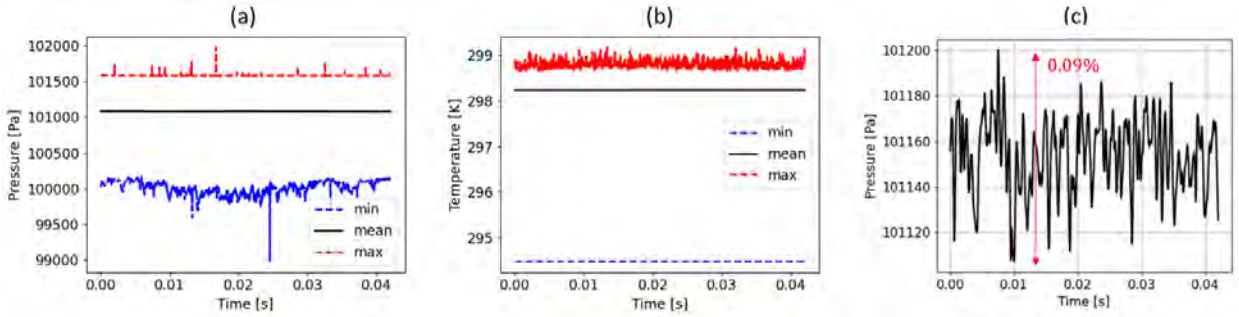

Figure 3 Convergence - (a)/(b) : time evolution of maximum, mean and minimum values for (a) global pressure and (b) temperature; (c) : pressure signal on the blade SS at midspan.

next sections. On the suction side, the effect of the trip that produces a random turbulence on the blade is also visible in both cases. Note that the transition to turbulence is not uniform in either case, but both simulations become full turbulent close to the blade trailing edge.

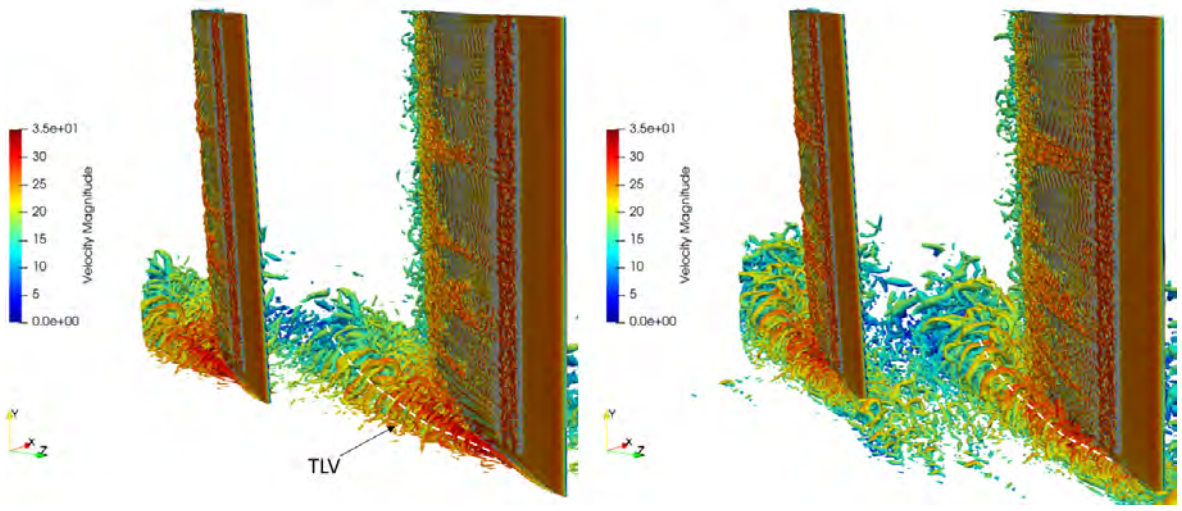

Figure 4 Isosurfaces of Q-criterion ($1.0x10^6\ s^{-2}$) coloured by the velocity magnitude - (left): moving end-wall; (right): fixed end-wall.

In Fig. 4, the turbulence development on the end-wall is different between the two cases as the local Reynolds number is higher in the stationary end-wall case. Indeed, the hairpin vortices that appear in front of the LE in the case with the stationary end-wall do not form in the current case, where the wall velocity has a strong component aligned with the inflow velocity that delays the boundary layer development and transition at the wall in front of the blade, as suggested by the

boundary layer parameters evaluated at $X/c_a = -0.1$ and $Z/c_a = 1.22$ shown in table 1. Moreover, the boundary layer profile on the lower wall is still non representative of a fully turbulent boundary layer and does not match the LES profile of You et al. (2007*a*) and that of the experiment (Wang and Devenport, 2004) close to the wall, as shown by the streamwise velocity profiles in Fig. 5 at $X/c_a = 0$ and $Z/c_a = 0$. In fact, as in the previous study (Koch et al., 2021*a*), the upstream trip on the plate has not been included in the present simulation to prevent an additional spurious noise source. However, as shown in the next sections, this mismatch doesn't provide strong differences in the mean flow neither inside of the passage nor downstream of the cascade. Finally, the acceleration shown by the velocity profile in the case with the stationary end-wall is due to the passage area restriction caused by the TLV, which spreads more in the spanwise direction, as described in the next sections.

BL parameters	LES moving	LES fixed
δ [mm]	8.56	7.64
δ^* [mm]	1.86	1.7
θ [mm]	1	1.1
H	1.86	1.55
Re_θ	732	769

Table 1 Boundary layer parameters at $X/c_a = -0.1$ and $Z/c_a = 1.22$ for the cases with and w/o sliding end-wall.

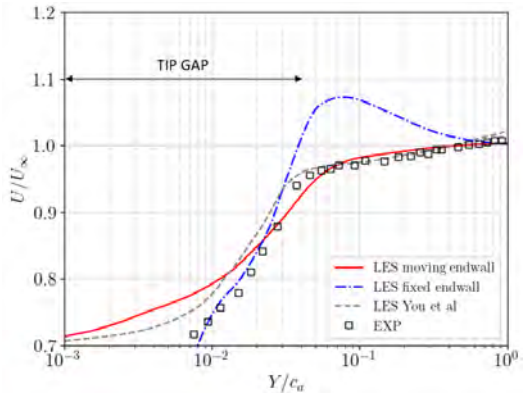

Figure 5 Profiles of the mean streamwise velocity at $X/c_a = 0$ and $Z/c_a = 0$.

In Fig. 6, similar iso-surfaces of Q-criterion but coloured by the streamwise vorticity are shown on the blade PS. A different behaviour in the boundary layer development close to the blade LE is found between the cases with and without end-wall motion: the thin laminar separation bubble at the leading edge develops slightly differently, which triggers an earlier transition to turbulence over most of the span in the stationary end-wall case. This, in turn, can be explained by the mean spanwise velocity contours shown in a vertical plane (A) perpendicular to the chord in Fig. 7 for the two cases. The area close to the external part of the vortex is characterized by high values of the vertical velocity with respect to the nearby regions. The TLV induces a radial flow that affects the transition of the boundary layer on the PS. In the moving end-wall case, more spots and a big area close to the tip are affected by the delayed transition (black arrows in Fig. 7) because of three different factors. First, the TLV coming from the adjacent blade is closer to the PS because of its trajectory. Secondly, the suction effect of the tip flow is increased by the wall motion, so that a stronger radial flow is induced on the PS. Finally, the incoming turbulent structures at the lower plate in front of the blade speed up the transition of the boundary layer interacting with the PS close to the tip in the case without the sliding end-wall.

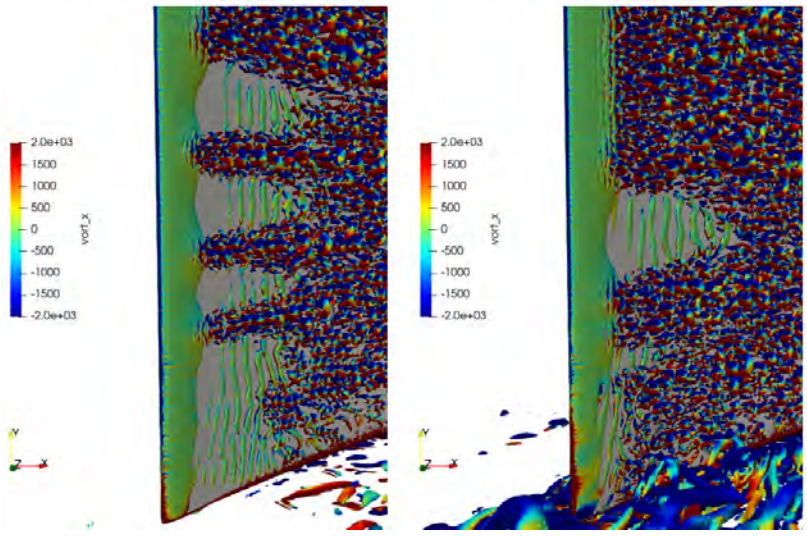

Figure 6 Iso-surfaces of Q-criterion ($1.0x10^6\ s^{-2}$) on the blade PS at the tip close to the LE: boundary layer development - (left): moving end-wall; (right): stationary end-wall.

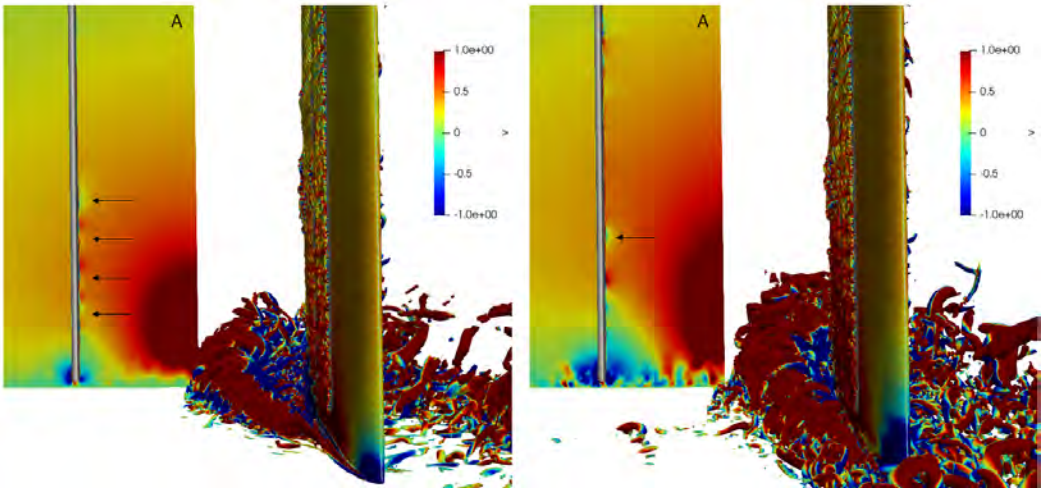

Figure 7 Mean spanwise velocity contour at plane A and interaction with the TLV - (left): moving end-wall; (right): stationary end-wall.

0.2 Aerodynamic performances

The pressure coefficient defined as $C_p = (P - P_\infty)/(0.5\rho U_\infty^2)$ is plotted against the normalized axial position in Fig 8 at midspan and near the tip region. The reference values are $P_\infty = 101160\ Pa$, $\rho = 1.225\ kg/m^3$ and $U_\infty = 25.5\ m/s$. The present LES is compared with the high-fidelity simulation by Koch et al. (2021*a*) and You et al. (2004), as well as with the available measurements in Wang and Devenport (2004). First, a global good agreement is obtained at midspan, which is far enough to be strongly affected by the effects of the end-wall motion. However, some differences can be seen on the pressure side very close to the leading edge, where the current LES better matches the experiment of Devenport *et al*. in the prediction of the laminar separation bubble, which was not captured in any previous high-fidelity simulations. The pressure coefficient distribution is well captured on both SS and PS. Some discrepancies are still visible at the LE and TE, where the incidence and the operating point probably don't match the experiment perfectly. Moreover, the local mismatch between the LES and the experiment, visible until $X/c_a = 0.1$, is also due to the trip width, which is not the same as in Wang and Devenport (2004). Yet, measurements by Muthanna (2002) showed that the flow downstream of the cascade was independent of the form and extent of the trip. Additionally, the two LES with and without wall motion are perfectly consistent and can thus be compared. Finally, due to the non physical behaviour of the C_p directly extracted on the trip, this region has been removed from the plot. Despite the differences discussed above, the blade loading at midspan globally

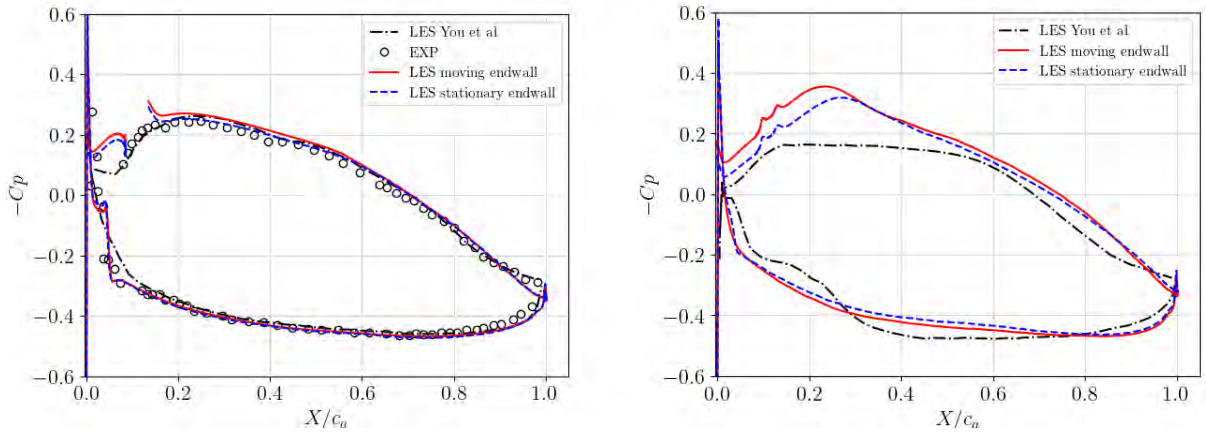

Figure 8 Pressure coefficient evaluated at midspan (left) and at 10%C_a away from the blade tip (right).

maintains the same distribution between the three simulations and the experiments. The pressure coefficient evaluated at the blade tip region shows a significantly different behaviour between the various cases. The result at the tip is strongly affected by the interaction of the blade with the incoming boundary layer at the wall, as suggested by the different pressure distribution of You et al. (2004). Therefore, an increased loading at the tip is obtained in the two current LES. Note that no experimental data are available at this spanwise location.

The friction coefficient C_f is plotted in Fig. 9 and compared once again with the stationary case. No significant differences are seen neither on the SS nor on the PS. The wall shear stress considered for the calculation of C_f takes into account all components and not only the one along the streamwise direction. For this reason, the local drop in the front part of the blade PS (X/c_a=0.05) which represents the laminar separation bubble still shows slightly positive values of the friction coefficient because of the induced radial flow shown in Fig. 7.

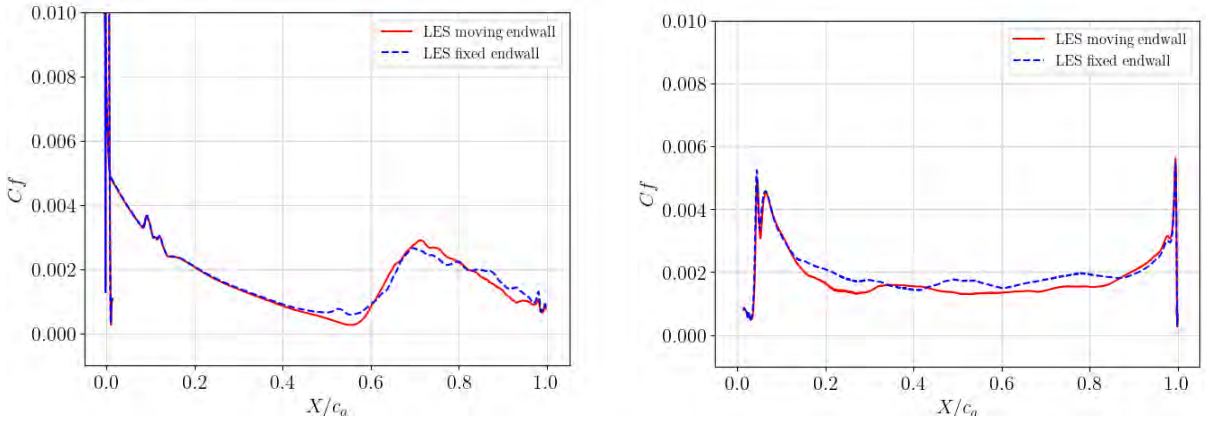

Figure 9 Friction coefficient evaluated at midspan at the blade SS (left) and PS (right).

0.3 Tip leakage vortex and wake description

Two cuts have been performed downstream of the cascade in the (Y,Z) planes at $X/c_a = 1.37$ and $X/c_a = 2.06$ respectively. The mean axial velocity normalized by the inflow velocity shown in Fig. 10 is compared with the the stationary end-wall case at the same locations. The wake and the TLV are identified and characterized by a strong deficit in the mean

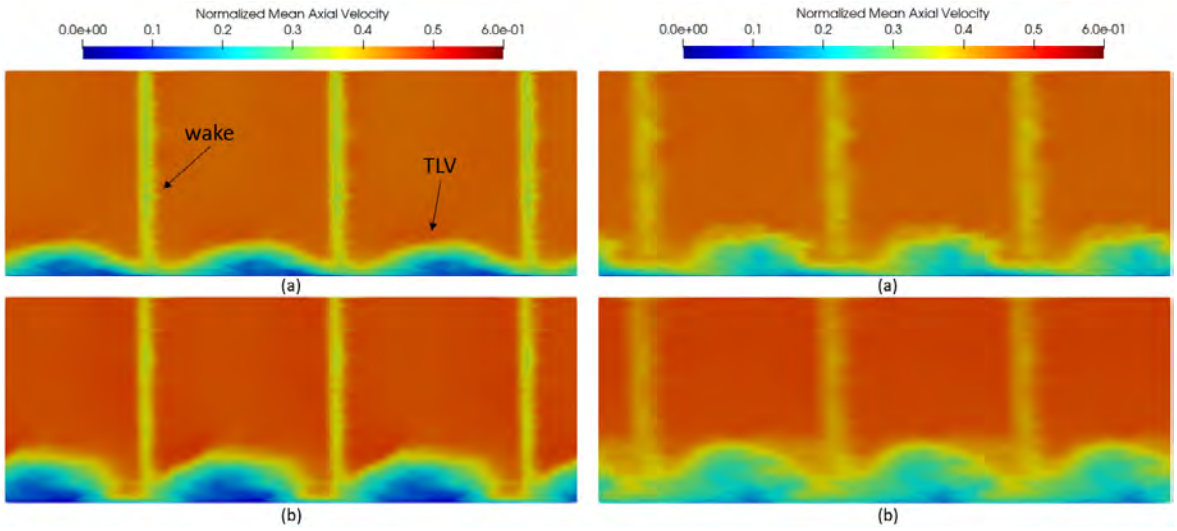

Figure 10 Normalized mean axial velocity at $X/c_a = 1.37$ (left) and $X/c_a = 2.06$ (right) - (a): moving end-wall (b): stationary end-wall.

axial velocity. The presence of the lower plate moving in the negative Z direction affects the shape and the development of the TLV. Indeed, the vortex is flattened towards the wall and stretched toward the next blade by the wall motion. The same observations were made by Wang and Devenport (2004).

Turbulent kinetic energy (TKE) normalized by the square of the inflow velocity at planes $X/c_a = 1.37$ and $X/c_a = 2.06$ is then shown in Fig. 11. Usually the TLV is characterized by a high turbulence region that borders the vortex. This is due to the axial velocity gradient that exists between the vortex and the main flow. In the presence of the wall motion the distribution of the turbulent kinetic energy again shows a shift to the right and a flattening of the tip leakage vortex as seen in the mean axial velocity contours. However, the TLV still has the upper region characterized by high turbulence levels. Compared to the stationary case, the high-turbulence region is narrower and less spread with two distinct peaks. As the

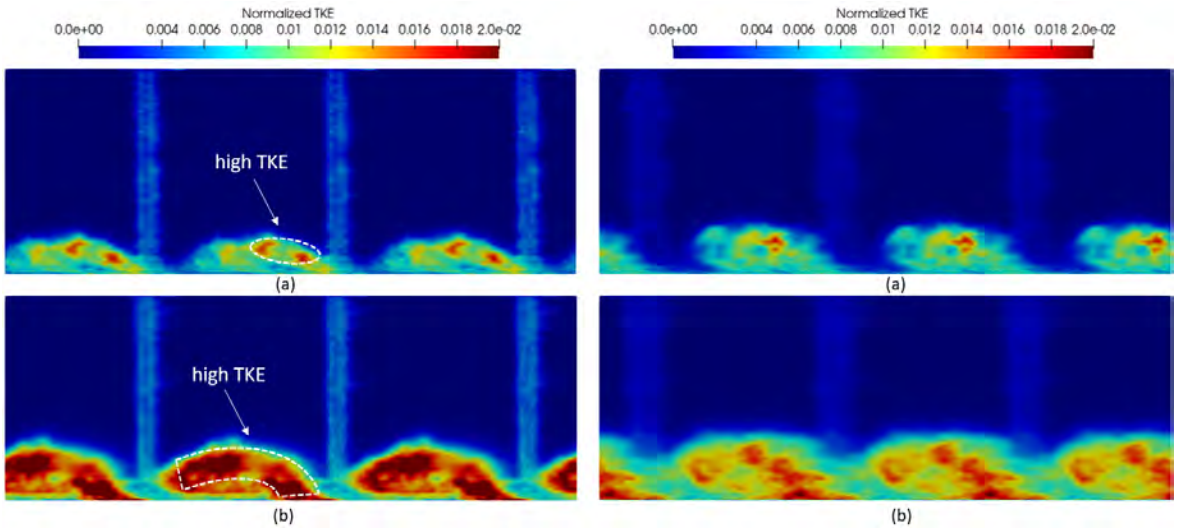

Figure 11 Normalized turbulent kinetic energy at $X/c_a = 1.37$ (left) and $X/c_a = 2.06$ (right) - (a): moving endwall (b): stationary endwall.

wall motion direction is well aligned with the external velocity of the vortex (positive X-vorticity), the velocity gradient at the wall is much smaller with respect to the case with the stationary end-wall. Therefore, the vortex shows lower turbulent kinetic energy levels. Moreover, the corresponding peak levels of TKE are about 45% lower with the presence of the moving wall, that is quite close to the 40% reduction measured by Wang and Devenport (2004).

To further characterize the TLV inside of the passage, isolines of normalized mean vorticity magnitude, defined as $|\Omega|c/U_\infty$, are illustrated in Fig. 12 for two (Y,Z) planes at $X/c_a = 0.5$ and $X/c_a = 0.7$ within the blade passage. The shape of the vortex is in good agreement with You et al. (2004) as well as the values obtained for the normalized vorticity. The flattening and entrainment effect of the wall is clearly visible even in the passage, as also suggested by the TLV trajectories described below.

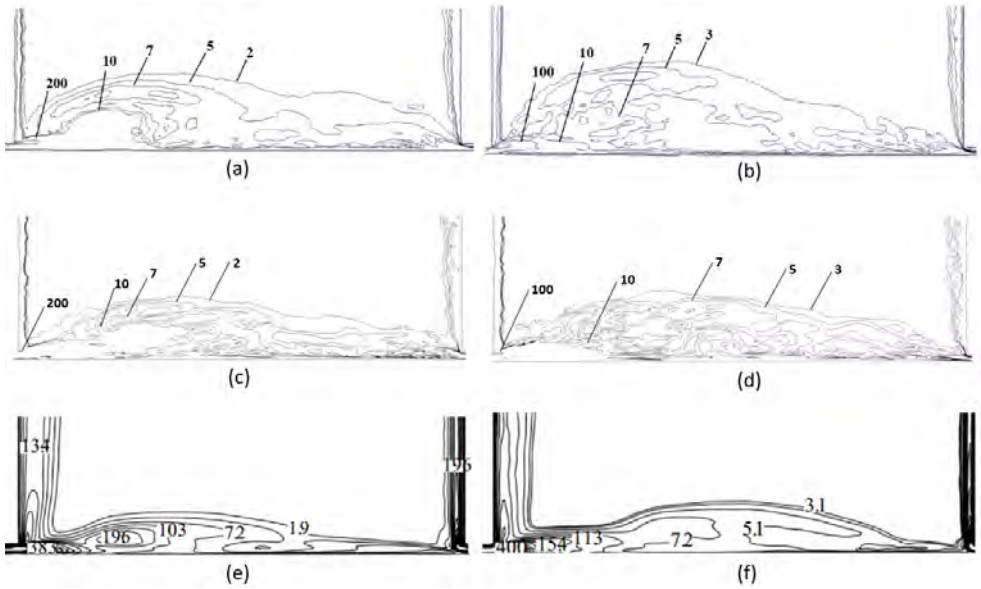

Figure 12 Iso-lines of normalized mean vorticity magnitude. Comparison between LES by Koch (above), present LES (middle) and LES by You et al (below) - (a)/(c)/(e): $X/c_a = 0.5$ and (b)/(d)/(f): $X/c_a = 0.7$.

Finally, the trajectories of both the wake and TLV are plotted in Fig. 13. The wake trajectory is obtained considering the peak of the mean axial velocity deficit at midspan and the results show a good agreement with respect to the experiments and the previous LES simulations, meaning that the wake is not affected at midspan by the wall motion. Then, the center of the TLV has been tracked with the maximum of the mean helicity (scalar product between velocity and vorticity) in the vortex region until the blade TE. An example is shown in Fig. 14, where mean helicity contours are shown at $X/c_a = 0.4$ for the two cases. Downstream of the cascade the vortex center cannot be identified anymore due to the coarser grid and

the previous criterion no longer gives a unique solution in the presence of the sliding wall. Therefore, the maximum of the streamwise velocity deficit in the vortex region has been chosen as the new more robust criterion, as it provides the same results in the cascade channel and a single solution downstream. The detachment point of the TLV from the blade SS remains the same for the two cases with and without the motion of the end-wall, but the vortex is clearly shifted toward the next blade in the streamwise direction with the moving end-wall. The resulting trajectory is also well aligned with the one obtained by You et al. (2004) and follows the experimental trend.

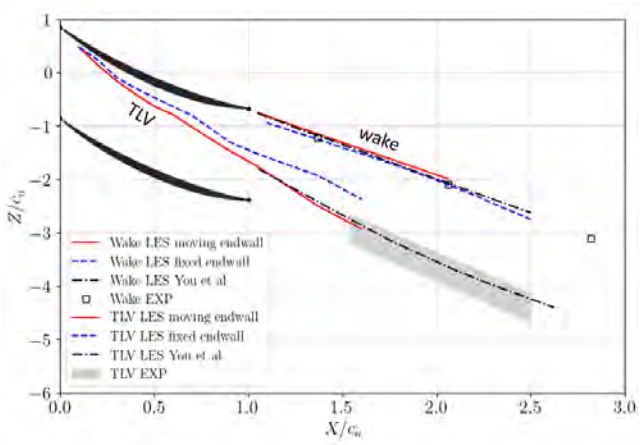

Figure 13 Tip leakage vortex and wake trajectories on the (X,Z) plane.

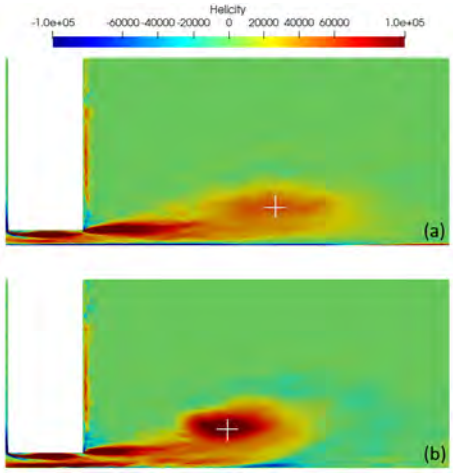

Figure 14 Mean helicity contours in the TLV region at $X/c_a = 0.4$ - (a): moving end-wall; (b): fixed end-wall.

CONCLUSIONS

A first wall-resolved compressible LES has been performed on a linear compressor cascade with tip-gap and a sliding end-wall in order to investigate the effects of the latter on the aerodynamic behaviour of the main flow structures that form, such as the tip-leakage vortex and the wake. The results have been compared with a previous LES on the same configuration with a stationary end-wall. The blade loading obtained at midspan is in good agreement with a previous incompressible LES and the experiments performed on the same cascade, while the differences at the tip are most likely caused by the incoming boundary layer, which is still laminar with a moving end-wall. Nonetheless, this mismatch does not affect the mean flow in the passage or downstream of the blade. With the moving wall, the TLV size, intensity, location and trajectory are also consistent with both the measurements from Muthanna and Devenport (2004); Wang and Devenport (2004) and the incompressible LES results of You et al. (2004).

The end-wall motion has a clear effect on the tip-leakage vortex characteristics, flattening and entraining the vortex towards the adjacent blade PS. It also triggers lower levels of turbulent kinetic energy, and the TLV extends less inside the passage in the spanwise direction. On the other hand, the wake trajectory downstream of the blade is not affected by the end-wall motion. Moreover, the new trajectory of the tip-leakage vortex together with an increased suction effect due to the tip-gap flow have been found to induce a radial flow on the blade PS. This seems to affect the boundary layer development and the turbulent breakdown close to the leading edge where the laminar separation bubble forms. As a next step, the effects of the moving end-wall on the cascade far-field noise will be achieved, as the tip-noise sources are expected to be influenced by the changes in the tip-gap flow.

References

Becherucci, L., Koch, R. and Moreau, S. (2022), 'Wall-resolved les of a linear compressor cascade with moving endwall', *28th AIAA/CEAS Aeroacoustics Conference* .

Denton, J. (1993), 'Loss mechanisms in turbomachines', *ASME 1993 Interantional Gas Turbine and Aeroengine Congress and Exposition* .

Donea, J. (1984), 'A taylor-galerkin method for convective transport problems', *International Journal for Numerical Methods in Engineering* **20**(1), 101–119.

Jacob, M. C., Grilliat, J., Camussi, R. and Gennaro, G. C. (2010), 'Aeroacoustic investigation of a single airfoil tip leakage flow', *International Journal of Aeroacoustics* **9**(3), 253–272.

Kameier, F. and Neise, W. (1997), 'Experimental study of tip clearance losses and noise in axial turbomachines and their reduction', *Journal of Turbomachinery* **199**(3), 460–471.

Kholodov, P. and Moreau, S. (2020*a*), 'Identification of noise sources in a realistic turbofan rotor using Large Eddy Simulation', *Acoustics* **2**, 691–706.

Kholodov, P. and Moreau, S. (2020*b*), Tip flow evolution in a turbofan rotor for broadband noise diagnostic, *in* '26^{th} AIAA/CEAS Aeroacoustics Conference', AIAA2020-2521 paper, Reno, NV.

Koch, R., Sanjose, M. and Moreau, S. (2021*a*), 'Aerodynamic investigation of a linear cascade with tip gap using large-eddy simulation', *Journal of the Global Power and Propulsion Society* **5**, 39, 49.

Koch, R., Sanjose, M. and Moreau, S. (2021*b*), 'Large-eddy simulation of a linear compressor cascade with tip-gap: aerodynamic and acoustic analysis', *AIAA Aviation 2021 Forum* .

Moreau, S. (2022), 'The third golden age of aeroacoustics', *Physics of Fluids* **34**(3), 031301:1–15.

Muthanna, C. (2002), 'Effects of free stream turbulence on the flow through a compressor cascade', *Ph.D. Dissertation* .

Muthanna, C. and Devenport, W. (2004), 'Wake of a compressor cascade with tip gap, part 1: Mean flow and turbulence structure', *AIAA Journal* **42**(11), 2320, 2331.

Nicoud, F. and Ducros, F. (1999), 'Subgrid-scale stress modelling based on the square of the velocity gradient tensor', *Flow, turbulence and Combustion* **62**(3), 183–200.

Odier, N., Sanjosé, M., Gicquel, L., Poinsot, T., Moreau, S. and Duchaine, F. (2019), 'A characteristic inlet boundary condition for compressible, turbulent, multispecies turbomachinery glows', *Computer & Fluids* **178**, 41–55.

Poinsot, T. J. and Lelef, S. (1992), 'Boundary conditions for direct simulations of compressible viscous flows', *Journal of computational physics* **101**(1), 104–129.

Schönfeld, T. and Rudgyard, M. (1999), 'Steady and unsteady flow simulations using the hybrid flow solver avbp', *AIAA Journal* **37**(11), 1378–1385.

Storer, J. and Cumpsty, N. (1993), 'An approximate analysis and prediction methodfor tip clearance loss in axial compressors', *Journal of Turbomachinery* .

Wang, Y. and Devenport, W. (2004), 'Wake of a compressor cascade with tip gap, part 2: Effects of endwall motion', *AIAA Journal* **42**(11), 2332, 2340.

Wenger, C., Devenport, W., Wittmer, K. and Muthanna, C. (2004), 'Wake of a compressor cascade with tip gap, part 3: Two-points statistics', *AIAA Journal* **42**(11), 2341, 2346.

Wisler, D. C. (1977), 'Core compressor exit stage. volume i - blading design', *NASA-CR-135391* .

You, D., Mittal, R., Wang, M. and Moin, P. (2004), 'Computational methodology for large-eddy simulation of tip-clearance flows', *AIAA Journal* **42**(2), 271–279.

You, D., Wang, M., Moin, P. and Mittal, R. (2006), 'Effects of tip-gap size on the tip-leakage flow in a turbomachinery cascade', *Physics of Fluids* **18**(10), 105102.

You, D., Wang, M., Moin, P. and Mittal, R. (2007*a*), 'Large-eddy simulation analysis of mechanisms for viscous losses in a turbomachinery tip-clearance flow', *Journal of Fluid Mechanics* **586**, 177–204.

You, D., Wang, M., Moin, P. and Mittal, R. (2007*b*), 'Vortex dynamics and low-pressure fluctuations in the tip-clearance', *Journal of Fluids Engineering, Transactions of the ASME* **129**(8), 1002–1014.